Daniel A. Bishop and Anthony Yezzi, "A simple shape prior model for iris image segmentation", Proc. SPIE 8029, Sensing Technologies for Global Health, Military Medicine, Disaster Response, and Environmental Monitoring; and Biometric Technology for Human Identification VIII, 80291T (2011).

A simple shape prior model for iris image segmentation

Daniel A. Bishop[a] and Anthony Yezzi, Jr.[b]

[a]Georgia Institute Of Technology, Atlanta, GA 30332, USA;
[b]Georgia Institute of Technology, Atlanta, GA 30332, USA

ABSTRACT

In order to make biometric systems faster and more user-friendly, lower-quality images must be accepted. A major hurdle in this task is accurate segmentation of the boundaries of the iris in these images. Quite commonly, circle-fitting is used to approximate the boundaries of the inner (pupil) and outer (limbic) boundaries of the iris, but this assumption does not hold for off-axis or otherwise non-circular boundaries. In this paper we present a novel, foundational method for elliptical segmentation of off-axis iris images. This method uses active contours with constrained flow to achieve a simplified form of shape prior active contours. This is done by calculating a region-based contour evolution and projecting it upon a properly chosen set of vectors to confine it to a class of shapes. In this case, that class of shapes is ellipses. This serves to regularize the contour, simplifying the curve evolution and preventing the development of irregularities that present challenges in iris segmentation. The proposed method is tested using images from the UBIRIS v.1 and CASIA-IrisV3 image data sets, with both near-ideal and off-axis images. Additional testing has been performed using the WVU Off Axis/Angle Iris Dataset, Release 1. By avoiding many of the assumptions commonly used in iris segmentation methods, the proposed method is able to accurately fit elliptical boundaries to off-axis images.

Keywords: biometrics, iris, segmentation, active contours, shape prior, off-axis

1. INTRODUCTION

Iris recognition is a growing form of biometric authentication. Though there is some variation, most published iris recognition methods follow the same general four-step process.[1–3] These steps are image capture, iris localization and segmentation, template generation, and template comparison. Each of these steps presents its own set of challenges, and each depends on the steps that come before.

One challenge in the image capture process is balancing the need for high-quality images with the comfort and ease of the user. A high-quality image features an iris clearly presented, looking directly at the camera, with little occlusion of the iris area by eyelashes and eyelids. Such images are difficult to capture and require cooperation on the part of a trained user. Iris recognition systems often expect and account for occlusion of the top and bottom portions of the iris in a captured image, but can encounter difficulty localizing an iris in an image that is off-axis, poorly centered, or heavily occluded.

The suitability of off-axis iris images for recognition purposes has been discussed in existing literature.[4,5] As expected, an off-axis image does not perform as favorably as an on-axis image in terms of recognition. However, it is not a hopeless case. Even image correction via a simple affine transform can allow for iris recognition with empirically estimable accuracy. Much of this research has been performed by manually segmenting off-axis images.[5] The time-consuming nature of manual segmentation has thus been a barrier in such research. The development of improved off-axis iris segmentation schemes will better allow for more accurate estimation of the effects of this form of image noise on recognition and allow for more robust performance in future iris recognition systems. This paper presents a new, less-constrained iris segmentation algorithm to handle off-axis and otherwise sub-optimal images.

Further author information: (Send correspondence to Daniel Bishop)
Daniel A. Bishop: dabishop@ece.gatech.edu
Portions of the research in this paper use the CASIA-IrisV3 collected by the Chinese Academy of Sciences Institute of Automation (CASIA).

2. TECHNICAL BACKGROUND

Any iris segmentation algorithm will require assumptions to be made about the characteristics of the captured image. Proposed segmentation algorithms commonly make assumptions based on iris and pupil shape, size, location within the image domain, et cetera. However, in order to segment lower quality iris images many of these assumptions must be relaxed. It is well-established that the inner (pupil) and outer (limbic) boundaries of the iris may not be perfectly circular even in images with no off-axis gaze, yet the circular Hough transform is commonly used even in segementers designed with off-axis images in mind. This can lead to sub-optimal boundary determination, as irregular boundaries are approximated with circles. Many methods also rely on specular reflection to be present within or near the pupil for localization purposes. This assumption does not necessarily hold in the case of off-axis images. The goal of this research is to minimize these traditional assumptions to segment images not generally handled by existing methods.

In recent years, active contour models have been proposed for iris segmentation with some success. For an image with intensity I on domain $\Omega \subset \mathbb{R}^2$, let $p \in [0,1]$ and $C(p) : [0,1] \to \Omega$ be a contour (function). This contour C will be used to demarcate the boundary in image segmentation. Give C some initial position $C(p,0)$ at time $t = 0$, with $C(p,t)$ varying with time.

With a function C and domain Ω, we can define an Energy Functional $E(C(t)) : \Omega \to \mathbb{R}$. E is generally calculated based upon characteristics of both contour C and image I. Ideally, E will be selected so that it is minimized when C corresponds to the desired segmentation boundary in Ω. At $t = 0$, $C(t)$ is not likely to be on that boundary. Thus, $C(t)$ is evolved with time by means of a gradient descent. That is, $\frac{\partial C}{\partial t} = -\nabla E$. This process was laid out by Kass, Witkin, and Terzopolous,[6] and refined by Osher and Sethian.[7]

The Energy Functional generally consists of two portions: an external energy term, which is dependent upon characteristics of the image I, and an internal energy term, which is dependent only upon $C(t)$. The external energy term in E may be based upon localized characteristics such as edge intensity, as with the original Snakes model,[6] or region-based characteristics, such as the Mumford Shah Energy.[8,9] The method presented here is region-based.

The internal energy term is a regularization term, generally designed to minimize arc length and prevent the development of sharp corners. This serves two purposes. First, it allows portions of the contour near regions that minimize E to influence parts of the contour that are not strongly controlled by the image-based portion of E. Second, it prevents the contour from being too strongly influenced by noise and local features in the image and becoming excessively jagged.

This internal regularization term can cause difficulty in iris segmentation. By their nature, Active Contours shrink, making them much better at being initialized outside of an object in question and contracting intward towards a boundary rather than being initialized inside of an object and expanding outward. However, since iris images generally contain more strong edges in the region outside of the iris and pupil than within it, an edge-based active contour generally must be initialized within the pupil/iris region. The active contour can be made to grow through a process called "ballooning,"[10] but this creates its own challenges, as the ballooning term can overcome the image-based energy and cause the contour to "leak" outside of the desired boundary. This method has been used for iris segmentation with some success,[11] but restricts the pupil to a circular boundary and, ultimately, uses a circular approximation of the limbic boundary for template generation.

In 2002, Chen, et al. described the use of shape prior active contour models.[12] These allow an active contour to be governed by a shape-based energy in addition to the internal and external energies. This method allows an active contour to estimate the boundaries of an object of known shape even in cases where the object is partially occluded. Unfortuantely, this method is computationally very expensive, requiring calculation of a signed distance function over large portions of the image domain. The proposed method is based upon a highly simplified form of shape prior active contours.

3. IMAGE PREPROCESSING

The first step in image preprocessing is to smooth any compression artifacts, if present. Several commonly-used iris image databases, including UBIRIS[13] and CASIA-IrisV3,[14] are distributed as JPEG-compressed images.

(a) Uncompressed Specularity (b) JPEG Specularity (c) Median Filtered JPEG Specular-
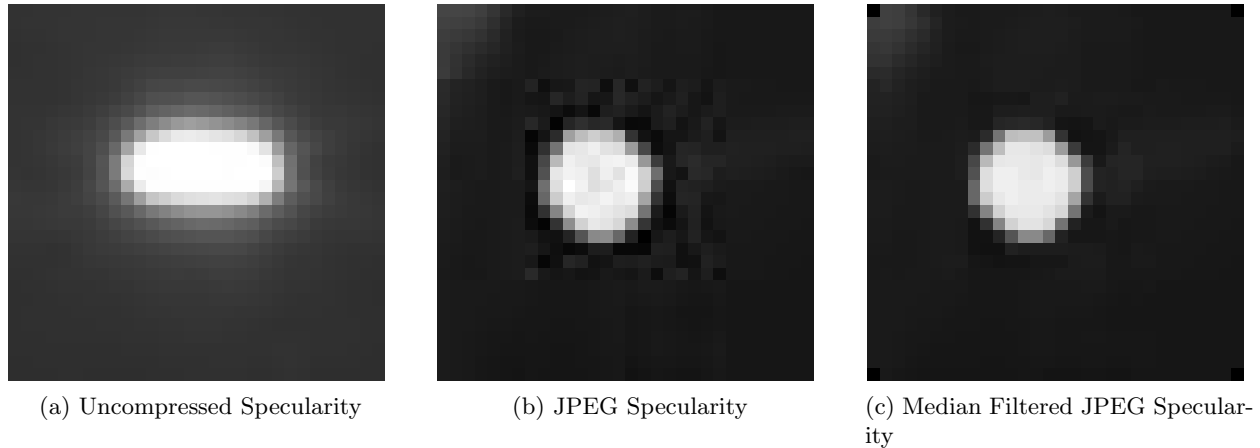ity

Figure 1: Compression artifacts are particularly apparent at specularities. This can affect specularity detection and removal. Median Filtering removes artifacts in the region, allowing it to respond better to morphological operations.

While the compression does not generally cause severe artifacting, there is generally some ringing surrounding particularly sharp edges, most notably surrounding illumination specularities commonly found in the pupil or iris regions, as seen in Figure 1. This ringing can interfere with thresholding and morphological operators used later. Thus, a 3x3 median filter is applied.

## 3.1 Inital Pupil Localization

Next, the pupil boundary contour is initialized. This is a very coarse localization, and is merely meant as a starting point for the pupil boundary contour rather than a final segmentation of it. The quality of this initialization affects the number of iterations the final segmenter must run to generate a final segmentation, but even a fairly poor initialization should be sufficient as long as some portion of the countour overlaps the pupil region. This is illustrated in Figure 2.

This initialization can be done any number of ways. One way is a simple region-growing routine. The image is binarized with a very low threshold value, and the number of regions is counted. The threshold is gradually raised until either the number of regions decreases, indicating the formation of a larger dark region in the image, or a predesignated threshold is met. Generally, during this process, the first large dark region to form as the merger of several smaller regions is the pupil. The pupil contour can then be initialized as a circle whose center is the centroid of the larger region and whose radius is either a predetermined guess or an estimate based upon the number of pixels in the region.

The method we use to initialize the pupil contour is actually a combination of the above and a coarse version of the shape prior active contours-based method used for final segmentation. First, the thresholding method is used to generate a binary image with a few dark regions. A large circular contour is then initialized on this binary image, just within the image bounds. This contour, C_{P_0} evolves according to a constrained flow with large step size to minimize the energy functional

$$E_{P_0} = \tfrac{1}{2}\left(u - v\right)^2.$$ (1)

Here, u is the mean intensity inside of C_{P0}, and v is the mean intensity outside. The contour does not evolve as a normal active contour, however. Rather, it evolves according to a constrained flow, maintaining its circular shape and varying with only three degrees of freedom: two of position and one of radius. This mechanism by which this is performed will be discussed in detail in Section 4. The pupil contour initialization process is demonstrated in Figure 3.
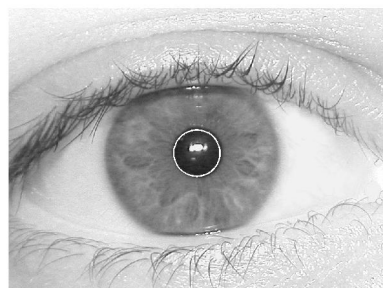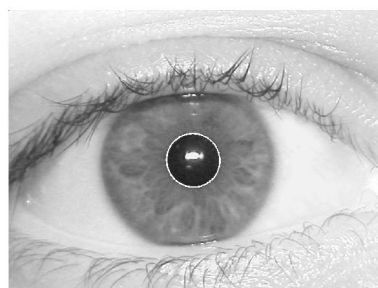
(a) Good Pupil Initialization
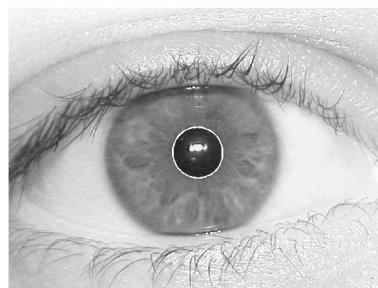
(b) Final Segmentation from (a)
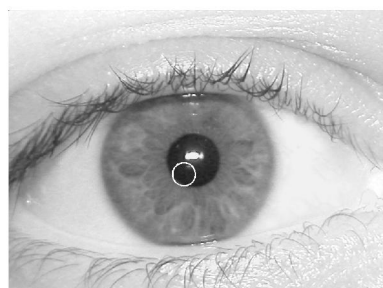
(c) Poor Pupil Initialization

(d) Final Segmentation from (c)

Figure 2: The output of the pupil contour initialization phase can can vary. Sometimes, it provides near-perfect segmentation, as in (a). In other instances, it provides only a poor approximation, as in (c). Within reasonable limits, a good final pupil segmentation can still be expected.

The energy functional in Equation 1, along with the imposed shape constraints, causes the contour to seek a region of pixels which are tightly-packed locally, rather than spread out in a narrow region, such as an eyebrow or eyelashes. Thresholding the image allows the use of a simpler energy functional and prevents the contour from getting caught in local minima.

The technique of dynamic thresholding and binary region-growing combined with a fast evolving contour to initially locate the pupil avoids some assumptions common in pupil localization. There is no assumption that the pupil is within a certain size range, beyond being larger than some small minimum. Additionally, there is no assumption about the location of the pupil within the image, though the contour may have difficulties with a pupil lying in an extreme corner of the image. There is also no assumption that a specularity will be present within the pupil region, or that the pupil within the image is circular. This last stament may seem strange, since C_{P_0} is defined to be restricted to a circle. However, this contour, as designed, will converge to a densely-packed dark region within the image regardless of shape.

3.2 Specularity Removal and Smoothing

The final pre-processing step in our system is to remove specularities that may be in the pupil or iris area and smooth the image. This is done by means of a morphological open and close.

Specularities are commonly found through thresholding. However, it is not uncommon for an iris image to include reflection in the skin area that saturate the camera sensor. This can cause large portions of the image to be considered specular reflections if thresholding is used. Additionally, JPEG-compressed images often have sharp edges smoothed or surrounded by ringing. This can lead to noise in the binary map created by thresholding.

As an alternative method, we use one-sided differencing to approximate the spatial derivative and detect specularities. Since the pupil and iris are generally the darkest regions of the eye, specularities in those regions
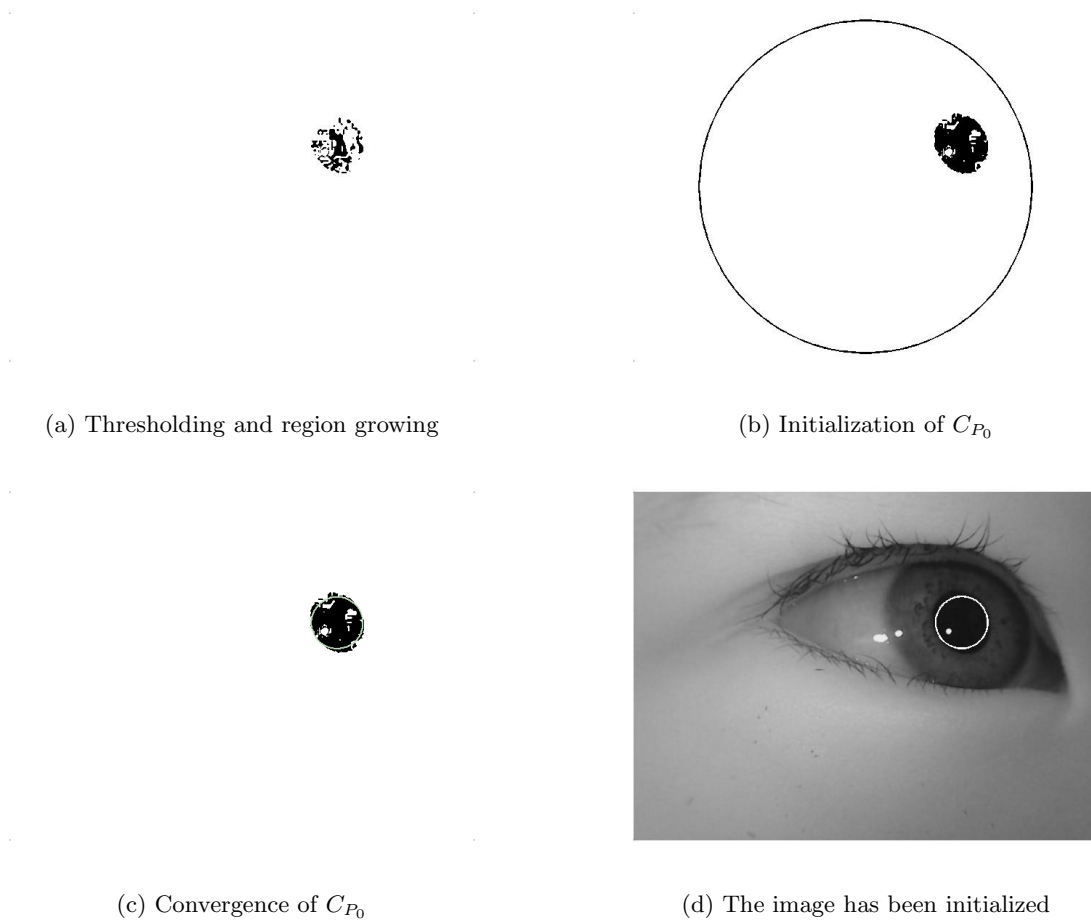
(a) Thresholding and region growing

(b) Initialization of C_{P_0}

(c) Convergence of C_{P_0}

(d) The image has been initialized

Figure 3: The above figures show the initialization process for contour C_{P_0}. First, the image undergoes region growing (a). Next, a contour is placed within the image and converges to the large region of dark pixels as seen in figures (b) and (c). The finished initialization is presented in figure (d)
.

present as spikes in the image gradient. The point on the image with the largest one-sided difference is located, and the local region is checked for the point with the most strongly negative one-sided difference. This process is performed in both the horizontal (x) and vertical (y) directions. This gives an estimate of specularity size. A circular structuring element of appropriate radius is then used in a morphological open followed by a morphological close.

The median filter applied to JPEG-compressed images described previously is useful during this process. If the median filter has not been applied, the image exhibits ringing surrounding any specularity. This is observable as a dark ring surrounding the specularity as seen in Figure 1b. Without the initial median filtering, the morphological processes would result in the specularities being replaced by very dark regions that can affect the contour evolution during the final segmentation process.

4. IRIS SEGMENTATION

As with the initial pupil localization described in Section 3.1, final segmentation of the pupil and iris is performed by means of a constrained flow and shape prior. The pupil boundary contour C_P is initialized to C_{P_0}, while the limbic boundary contour C_L is initialized to a circle centered upon and larger than C_P. Both C_P and C_L evolve simultanously. The pupil boundary contour will be discussed first:

$$E_P = -\frac{W_1}{2} \left(u_P - v_P\right)^2 + W_2 \left(\int_{R_P} \left(I - u_P\right)^2 + \int_{R_P^C} \left(I - v_P\right)^2 \right). \tag{2}$$

Here, R_P is the region contained within contour C_P and R_P^C is the complement. u_P and v_P are the image mean intensities in regions R_P and R_P^C, respectively. W_1 and W_2 are weighting terms, and I is the image intensity. The first term in this energy functional, when minimized, will maximize the difference between the means of the R_P and R_P^C.[15] The second term is the traditional Chan-Vese functional,[9] which, when minimized, divides the image into the optimal binary piecewise-constant partition. The first term causes C_P to enclose a small, dark region of the image. The second term prevents the contour from collapsing around a small, particularly dark region within the pupil that may be present.

There are only external energy terms in this functional, no regularization terms. Regularization is handled by constraining the evolution of C_P. Rather than evolve C_P as a free-flowing contour, it is forced to maintain the shape of an ellipse. As such, it can be completely defined by five parameters: horizontal center position, x_P; vertical center position, y_P; two radii, a_P and b_P, which define the eccentricity of the ellipse; and the angle of orientation, ϕ_P.

The functional in Equation 2 leads to the following flow:

$$F_P = \left[W_1 \left(u_P - v_P\right) \left(\frac{I - u_P}{A\left(R_P\right)} + \frac{I - v_P}{A\left(R_P^C\right)} \right) + W_2 \left(u_P - v_P\right) \left(I - \frac{u_P + v_P}{2} \right) \right] \vec{N}. \tag{3}$$

Here, $A\left(R_P\right)$ and $A\left(R_P^C\right)$ refer to the areas of the regions R_P and R_P^C, respectively, and $\vec{N}$ is the unit normal vector to C_P.

In practice, we actually use a slightly modified form of the Chan-Vese portion of the flow. Since, after the initial processing described in Section 3, the pupil region is relatively uniform, while the remainder of the image is more heterogeneous, we bias this term using a weight $\alpha \in [0, 1]$. This gives the curve flow

$$F_P = \left[W_1 \left(u_P - v_P\right) \left(\frac{I - u_P}{A\left(R_P\right)} + \frac{I - v_P}{A\left(R_P^C\right)} \right) + W_2 \left(u_P - v_P\right) \left(I - \alpha u_P - \left(1 - \alpha\right) v_P \right) \right] \vec{N}. \tag{4}$$

The limbic iris contour C_L is initialized as a circle outside of the initial location of the pupil contour. Like C_P, it is defined as an ellipse with corresponding parameters x_L, y_L, a_L, b_L, and ϕ_L. Its energy function is similar to the one in Equation 2, but contains terms dependent upon C_P.

$$E_L = -\frac{W_3}{2}\left(u_P - v_P\right)^2 + W_4 \left(\int_{R_L \setminus R_P} \left(I - u_L\right)^2 + \int_{R_L^C} \left(I - v_L\right)^2\right) + 10\left(\frac{a_P}{a_I}\right)^{25} + 10\left(\frac{b_P}{b_I}\right)^{25}. \tag{5}$$

Here, R_L is the region enclosed by C_L, R_L^C is the complement of this region. u_L is the mean of the image intensity in $R_L \setminus R_P$ and v_L is the mean intensity in R_L^C. W_3 and W_4 are weighting terms. Note that the region R_P is excluded from this energy functional. Additionally, there are terms based upon the radii of C_L and C_P. These terms prevent the contour C_L from collapsing upon C_P, as may occasionally happen in situations with poor initialization.

From Equation 5, we again modify the Chan-Vese term as in Equation 4 to get the following flow:

$$
\begin{aligned}
F_L = \Bigg[& W_3 \left(u_L - v_L\right)\left(\frac{I - u_L}{A\left(R_L\right)} + \frac{I - v_L}{A\left(R_L^C\right)}\right) + W_4 \left(u_L - v_L\right)\left(I - \beta u_L - \left(1 - \beta\right) v_L\right) \\
& + 250 \left(\frac{a_P}{a_L^2}\right)\left(\frac{a_P}{a_L}\right)^{24} + 250 \left(\frac{b_P}{b_L^2}\right)\left(\frac{b_P}{b_L}\right)^{24} \Bigg] \vec{N}.
\end{aligned}
\tag{6}
$$

Here, $\beta \in [0,1]$ serves to bias the Chan-Vese term, and $A\left(R_L\right)$ and $A\left(R_L^C\right)$ are the areas of R_L and R_L^C, respectively.

4.1 Shape Priors and Constrained Flow

As mentioned previously, none of the above energy functionals contain regularization terms. Rather, regularization is enforced by limiting the contours to a class of shapes. To accomplish this, the contour evolutions F_P and F_L are calculated at each timestep according to Equations 4 and 6 and used to calculate evolutions for each of the five ellipse parameters. The flow for each of these parameters is determined by the equation

$$g_t = \oint_C \vec{v_g} \cdot F \tag{7}$$

. Here, g_t is a placeholder for the time evolutions of each of the ellipse parameters x, y, a, b, and ϕ; $\vec{v_g}$ is the placeholder for the vector corresponding to each respective parameter; and $\vec{N}$ is the vector normal to the contour C. F is the curve evolution calculated through either Equation 4 or Equation 6. Vector $\vec{v_g}$ serves to constrain the flow of the contour to the appropriate dimension. For example, the vectors v_x and v_y for the position parameters x and y are very simple,

$$v_x = \begin{vmatrix} 1 \\ 0 \end{vmatrix}, \qquad v_y = \begin{vmatrix} 0 \\ 1 \end{vmatrix}. \tag{8}$$

Others, however, depend upon point $p = (p_x, p_y)$ on the contour, such as the ones for radii a and b:

$$v_a = \begin{vmatrix} \cos\left(\phi\right) \\ \sin\left(\phi\right) \end{vmatrix} \times \text{sign}\left(\left|\cos\left(\phi\right), \sin\left(\phi\right)\right| \times \begin{vmatrix} p_x - x \\ p_y - y \end{vmatrix}\right), \tag{9}$$

$$v_a = \begin{vmatrix} \cos\left(\phi + \frac{\pi}{2}\right) \\ \sin\left(\phi + \frac{\pi}{2}\right) \end{vmatrix} \times \text{sign}\left(\left|\cos\left(\phi + \frac{\pi}{2}\right), \sin\left(\phi + \frac{\pi}{2}\right)\right| \times \begin{vmatrix} p_x - x \\ p_y - y \end{vmatrix}\right). \tag{10}$$

5. RESULTS

We tested the proposed segmentation algorithm on images from the UBIRIS.v1 dataset[13] as well as a selection from the CASIA-IrisV3[14] database. The UBIRIS.v1 datased consists of full-color images captured in the visible spectrum and contain a variety of noise factors. The proposed segmentation algorithm was used on the red channel of each image. The CASIA-IrisV3 contains images captured at near-infrared (NIR) wavelengths, and test images were chosen for off-axis presentation and limited iris occlusion. Additional testing has been done on the WVU Off-Axis/Angle Iris Dataset.[16]

Though many noise factors were present, the proposed algorithm correctly fit elliptical pupil boundaries in 62% of the UBIRIS images tested. This was measured by visual inspection. Failure cases generally fell into four categories: large specularities, heavy blur, eyelash influence, and occlusion. These are illustrated in Figure 4. Performance was better for the WVU Off-Axis dataset, as the pupil boundary was correctly identified for 93% of images. For these images, failure cases were generally caused by either large specularities on the pupil-iris boundary or faulty initialization.

While other algorithms beat the proposed method on standard images with circular iris boundaries, the proposed method demonstrates its strength in accurately localizing pupil boundaries in off-axis and otherwise irregular cases. Example segmentation for near-ideal images is shown in Figure 5. Example segmentation for off-axis images is shown in Figures 6 and 7.

As expected, limbic boundary performance is poor for images that contain much eyelid occlusion. This is not surprising because, as described, the proposed method makes no allowance for pupil or iris occlusion. This will be one of the next steps in future development.

Evaluation of this scheme in comparison to existing iris segmentation methods presents some difficulty, as research on the proper normalization of off-axis iris images is still relatively young. It is the hope of the researchers that growing research in off-axis segmentation will assist in this development.

6. SUMMARY AND FUTURE WORK

Accurate iris segmentation is vital to successful iris recognition, and is a major obstacle to performing recognition using non-ideal images. This paper presents a novel segmentation scheme base upon a region-based shape prior active contour model and establishes its worth as an extensible foundation for future off-axis segmentation work. There is yet much work to do.

In future work we will allow for the effects of iris and pupil occlusion, broadening the class of images successfully segmented by this method. Additionally, the current process for initializing the pupil contour will be improved in future iterations for greater accuracy and efficiency. We also hope in the future to allow for the relaxation of curve constraints to allow for more degrees of freedom in the segmentation boundary, and to allow for the detection of eyelid boundaries. Additionally, we hope to investigate other means of differentiating image regions rather than intensity. In order to allow for this improved performance, constraints must be placed upon the input images. Great care must go into these decisions to allow for the segmentation of the widest possible class of iris images.

REFERENCES

1. Daugman, J. G., "Biometric personal identification system based on iris analysis." Patent (03 1994). US 5291560.
2. Daugman, J., "High confidence visual recognition of persons by a test of statistical independence," *IEEE Transactions on Pattern Analysis and Machine Intelligence* **15**, 1148–1161 (Nov. 1993).
3. Bowyer, K. W., Hollingsworth, K., and Flynn, P. J., "Image understanding for iris biometrics: A survey," *Computer Vision and Image Understanding* **110**, 281–307 (May 2008).
4. Daugman, J., "New methods in iris recognition," *IEEE Transactions on Systems, Man, and Cybernetics–Part B:Cybernetics* **37**, 1167–1175 (Oct. 2007).
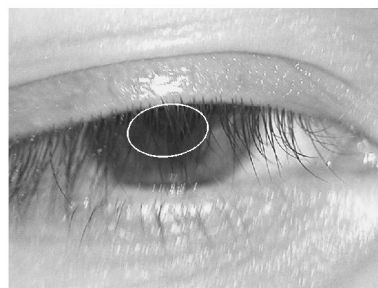
(a) Large Pupil Specularity
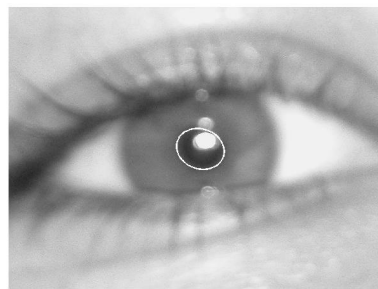
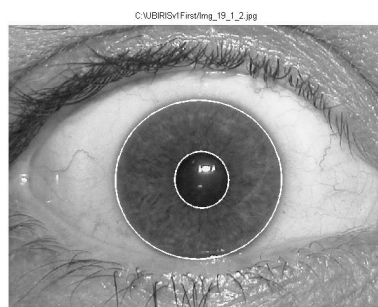(b) Heavy Blur
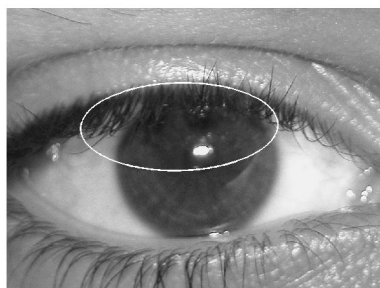
(c) Eyelash noise

(d) Occlusion

Figure 4: Several failure cases for pupil segmentation are presented here. Proportionally large specularities located within a pupil can sometimes not be properly filled during preprocessing, causing the contour to miss part of the pupil, as in (a). Figure (b) demonstrates what could be considered some scaling error in a poorly-focused image. Figure (c) demonstrates one of the risks of using a less-constrained segmentation system, as dark eyelashes severely distort the pupil boundary, and Figure (d) demonstrates the effect of occlusion on the segmenter.
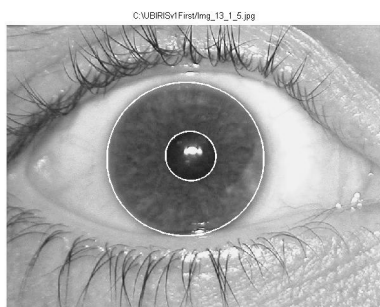
(a) Elliptical Iris Segmentation

(b) Elliptical Iris Segmentation

Figure 5: Near-ideal images segmented using the proposed method.
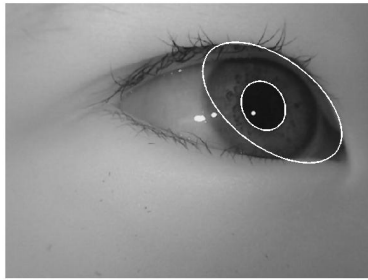
(a) Off-Axis Example
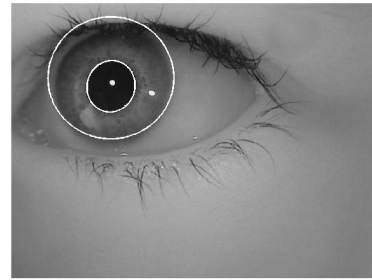
(b) Heavy Blur

Figure 6: Segmentation of off-axis images. Note that occlusion of the iris region in (a) causes severe distortion of the limbic boundary. Occlusion error in (b) is less severe.

5. Kennell, L. R., Broussard, R. P., Ives, R. W., and Matey, J. R., "Preprocessing of off-axis iris images for recognition," in [*Optics and Photonics for Counterterrorism and Crime Fighting IV*], Owen, G., ed., *Proceedings of the SPIE* **7119** (2008).

6. Kass, M., Witkin, A., and Terzopoulos, D., "Snakes: Active contour models," *INTERNATIONAL JOURNAL OF COMPUTER VISION* **1**(4), 321–331 (1988).

7. Osher, S. and Sethian, J. A., "Fronts propagating with curvature dependent speed: Algorithms based on hamilton-jacobi formulations," *JOURNAL OF COMPUTATIONAL PHYSICS* **79**(1), 12–49 (1988).

8. Mumford, D. and Shah, J., "Optimal approximations by piecewise smooth functions and associated variational problems," *Communications on Pure and Applied Mathematics* **42**(5), 577–685 (1989).

9. Chan, T. F. and Vese, L. A., "Active contours without edges," (1998).

10. Cohen, L. D., "On active contour models and balloons," (1991).

11. Shah, S. and Ross, A., "Iris segmentation using geodesic active contours," *Information Forensics and Security, IEEE Transactions on* **4**, 824 –836 (dec. 2009).

12. Chen, Y., Tagare, H. D., Thiruvenkadam, S., Huang, F., Wilson, D., Gopinath, K. S., Briggs, R. W., and Geiser, E. A., "Using prior shapes in geometric active contours in a variational framework," *International Journal of Computer Vision* **50**, 315–328 (2002). 10.1023/A:1020878408985.

13. Proença, H. and Alexandre, L., "UBIRIS: A noisy iris image database," in [*13th International Conference on Image Analysis and Processing - ICIAP 2005*], **LNCS 3617**, 970–977, Springer, Cagliari, Italy (September 2005).

14. "Casia-irisv3." http://www.cbsr.ia.ac.cn/IrisDatabase.

15. Yezzi Jr., A., Tsai, A., and Willsky, A., "A statistical approach to snakes for bimodal and trimodal imagery," *Computer Vision, 1999. The Proceedings of the Seventh IEEE International Conference on* **2**, 898 –903 vol.2 (1999).

16. "WVU: Off Axis/Angle Iris Dataset Collection." http://www.citer.wvu.edu/biometric_dataset_collections.
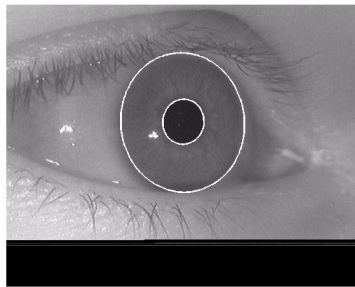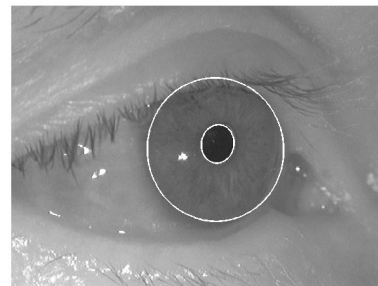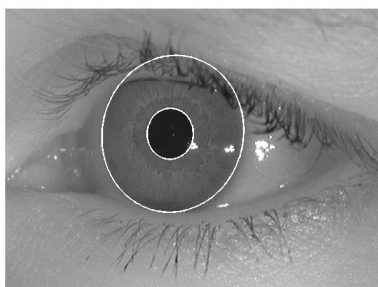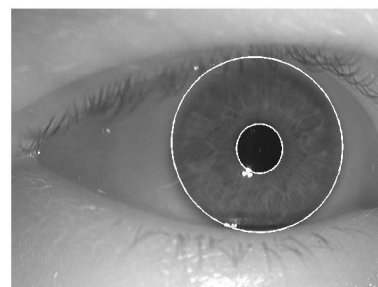
(a)
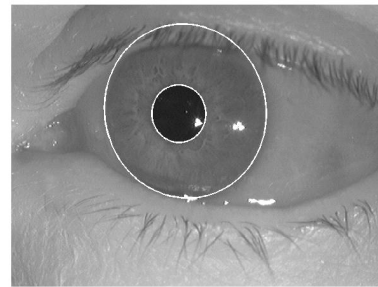
(b)
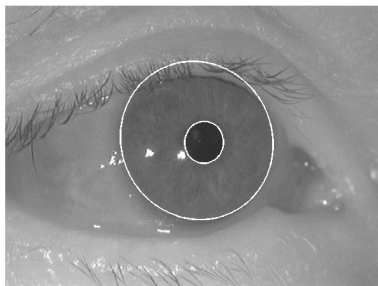
(c)

(d)

(e)

(f)

Figure 7: Segmentation of low-occlusion off-axis images.